RSC Advances

PAPER

View Article Online
View Journal | View Issue

Cite this: *RSC Adv.*, 2017, **7**, 29639

Investigation of carbon deposition induced by pyrolytic decomposition of ethylene

Ling Lin,[ac] Meishuang Lai,[b] Haifang Li,[b] Fei Tian,[a] Yulong Chen,*[d] Jiashu Sun*[ac] and Jin-Ming Lin*[b]

Received 16th April 2017
Accepted 29th May 2017

DOI: 10.1039/c7ra04282e

rsc.li/rsc-advances

Carbon deposition is an undesired side product, significantly inhibiting chemical reactions as well as leading to performance degradation. To efficiently prevent carbon deposition, the underlying mechanism needs to be elucidated. In this work, we have employed Raman spectroscopy to characterize the formed carbon deposits under different conditions inside a high temperature furnace heating system with a built-in U-shape quartz tube. The formation of graphite/amorphous carbon deposition was related to the temperature-dependent diffusion rate of carbon atoms, as well as the surface state of stainless steel. These investigations would help reduce unnecessary carbon deposition not only in ethylene but also in other industrial productions such as fuel cells.

1. Introduction

Carbon deposition from gas precursors is undesired but is significantly happening in a variety of industrial processes especially in the production of ethylene and its derivative products.[1–4] Carbon atoms deposited on the wall of vessels or in the catalyst significantly inhibit the reactions such as steam reforming, hydrogenation, methanation, and water gas shift *etc.*[5–8] The complex behaviors of carbon and hydrogen atoms would lead to the formation of undesirable byproducts along with desired products, and cause metal dusting. Therefore, investigating the formation mechanism of carbon deposition is beneficial for preventing its happening, which would help increase the product quality and meet the environmentally friendly requirement.

Raman spectroscopy is an effective tool for studying structure of carbon species, and its ability to distinguish different forms of carbon associated with chemical processes and environments is highly remarkable.[9–13] The Raman fingerprint of carbon is specially corresponding to its structural properties, thus capable of identifying the structural form of the deposited carbon. It has attracted much attention from scientists in the study of carbon materials including graphene, carbon nanotubes, carbon films, carbon deposits in fuel cell and carbon deposits derived from engine oil degradation.[14–16] Previous studies of carbon deposition based on Raman spectroscopy have been mainly focused on investigating the cathode, electrolyte, interconnects, anodes, and sealing materials as well as fuels.[16–20] Although some research groups have reported the morphologies and conditions of carbon deposition on metals such as Fe, Ni and Cr,[21–24] the underlying mechanism of carbon deposition on stainless steel, especially during the process of ethylene is still unclear. Stainless steel is a universal material used in industrial equipment such as engine combustor. However, the contents of 18% chromium and 8% nickel in stainless steel could act as the catalyst, while accelerating the side effect of carbon deposition.

In this work, to better understanding of the mechanism involved in carbon formation on stainless steel, we designed a system composed of a high temperature heating system conjunct with a U-shape quartz tube for collection of carbon deposits from ethylene gas (C_2H_4). The effects of position of stainless steel, temperature, flow rate of ethylene, and acid treatment of stainless steel were systemically investigated. The underlying mechanism of carbon deposition on stainless steel was proposed, which could provide insights into prevention of carbon deposition processes and optimization of product quality.

2. Experimental

2.1 Instruments

RM-2000 Raman spectroscopy (Renishaw, Gloucestershire, England) equipped with argon ion laser (514.5 nm) was used in the structural characterization of carbon deposits. Quanta 200 SEM (FEI, America) was employed in the surface topography

[a]*CAS Key Laboratory of Standardization and Measurement for Nanotechnology, CAS Center for Excellence in Nanoscience, National Center for Nanoscience and Technology, Beijing 100190, P. R. China. E-mail: sunjs@nanoctr.cn*

[b]*Beijing Key Laboratory of Microanalytical Methods and Instrumentation, The Key Laboratory of Bioorganic Phosphorus Chemistry & Chemical Biology, Department of Chemistry, Tsinghua University, Beijing 100084, P. R. China. E-mail: jmlin@mail.tsinghua.edu.cn*

[c]*University of Chinese Academy of Sciences, Beijing 100049, P. R. China*

[d]*Department of Hydraulic Engineering, Tsinghua University, Beijing 100084, P. R. China. E-mail: chen_yl@tsinghua.edu.cn*

analysis of carbon deposits. A special apparatus combined with high temperature furnace (Jinan Ximaden Technology Co. Ltd, Shandong, China) was designed for collection of carbon deposition. PHI Quantro SXM X-ray photoelectron spectroscopy (XPS) (ULVAC-PHI Inc., Japan) and X-ray diffraction (XRD) (Rigaku Corporation, Japan) were employed for investigation of the chemical state of metal element on stainless steel surface.

2.2 Chemicals and materials

Analytical pure reagents including ethanol, hexane, sulfuric acid (98% H_2SO_4), hydrochloric acid (98% HCl), sodium hydroxide (NaOH) and potassium dichromate ($K_2Cr_2O_7$) were purchased from Beijing Chemical Reagent (Beijing, China). Chromic acid lotion was prepared by the reaction among $K_2Cr_2O_7$, H_2SO_4 and H_2O. Stainless steel of no. 304 was commercially available and prepared as a substrate for carbon deposition by cutting to a size of 14 × 14 × 2 mm (length × width × height) in this work. Oil was removed from the surface of stainless steel with ethanol and hexane followed by washing with deionized (DI) water and drying. Ethylene gas (C_2H_4, 99.9% purity) and nitrogen gas (99.9% purity) were purchased from Beijing Hua Yuan Gas Chemical Industry Co. LTD. (Beijing, China). U-shape quartz tube was ordered from Beijing Jingqihui Quartz Products Co., LTD. (Beijing, China). All water used in this work was DI water.

2.3 Design of heating system for carbon deposition

To mimic the conditions of carbon deposition in industrial ethylene-related applications, an apparatus composed of a high-temperature heating furnace and a U-sharp quartz tube was designed (Fig. 1). Stainless steel of no. 304, one of the common materials used in engine combustor, was chosen as the substrate for carbon deposition. The U-sharp tube contained pipelines of two different sizes. The small pipeline is 6 mm in inner diameter, 8 mm in outer diameter, and 90 cm long. The large pipeline is 17 mm in inner diameter, 20 mm in outer diameter, and 75 cm long (Fig. 1). These two pipelines were devised for carrying N_2 and C_2H_4 gas. N_2 gas was used as carrier gas to drive air away from the heating system. The relatively small inner diameter of the pipeline was designed to increase the contact area and to shorten the reaction time in laboratory simulation. The sheets of stainless steel of no. 304 (14 × 14 × 2 mm) were placed into the bottom of long U-shape quartz tube at pre-determined positions before heating. When C_2H_4 continuously flowed into the designed pipeline inside the furnace, C_2H_4-induced carbon deposition on the surface of stainless steel occurred. The general carbon deposition mechanism was presented in Fig. 2. C_2H_4 was first adsorbed onto the surface of metal, while carbon atoms from C_2H_4 were dissolved and diffused into the metal, resulting in the formation of the metal carbides. The formed metal carbides further adsorbed C_2H_4, and carbon atoms were again dissolved and diffused into metal carbides. With the process continuously happened, the carbon deposition was growing.

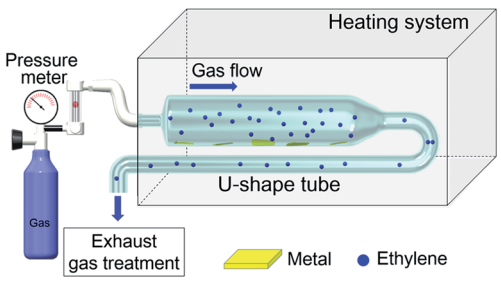

Fig. 1 An apparatus designed for the collection of carbon deposition when the interaction between C_2H_4 and stainless steel occurred inside a furnace.

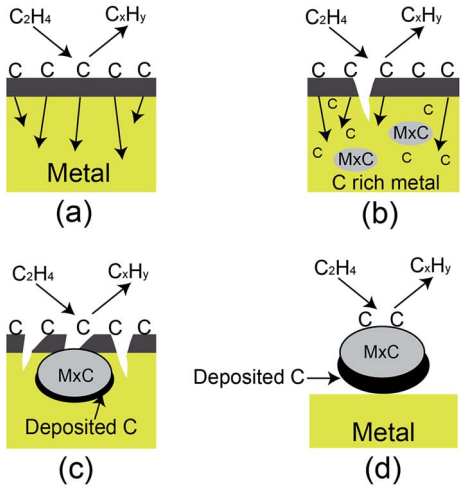

Fig. 2 The formation mechanism of carbon deposition onto the surface of stainless steel. Briefly, (a) C_2H_4 is desorbed onto the surface of metal, (b) carbon atoms from C_2H_4 are diffused into the metal to form the metal carbides, (c) the formed metal carbides adsorb more carbon atoms from C_2H_4, and (d) the carbon deposits grow.

3. Results and discussion

3.1 The effect of position, temperature and gas flow rate on carbon deposition

A variety of factors may affect the carbon deposition on stainless steel induced by C_2H_4 in the designed apparatus. These factors included the position of stainless steel inside the U-type quartz tube, the heating temperature inside furnace, the flow rate of C_2H_4, which were systematically studied as below.

To study the position effect of metal for carbon deposition, seven pieces of stainless steel were put into the U-type quartz tube with pre-determined positions. The first piece was placed near the inlet of tube, and the distance between two adjacent pieces was 5 cm. The tube with seven pieces of stainless steel inside was heated at 400 °C for 30 min, and the flow rate of C_2H_4 inside tube was 30 mL min^{-1}. After treatment, the stainless steel was carefully removed from the U-shape quartz, and the carbon disposition on the surface was characterized by Raman spectroscopy. Raman spectra showed four primary features at 1357 cm^{-1} (D-band), 1585 cm^{-1} (G-band), 2714 cm^{-1} (2D-band), and 2972 cm^{-1} (D + G-band), respectively. These four peaks

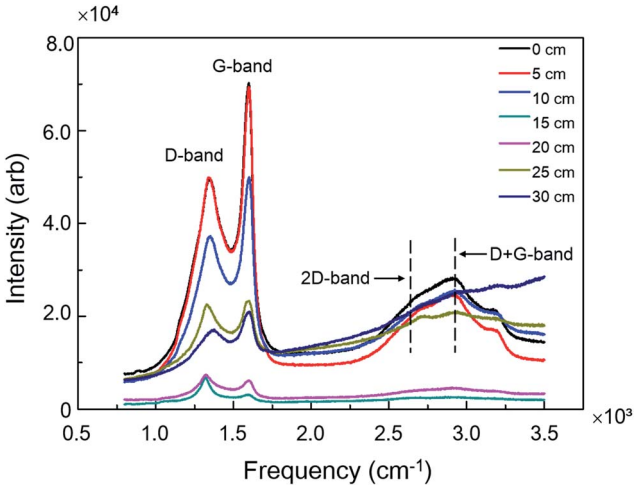

Fig. 3 Raman spectra of carbon deposited on the surface of stainless steel at different positions in U-type quartz tube.

illustrated that different carbon species were formed. D-band indicates the disordered structure of deposited carbon, attributed to the structural defects such as holes or impurities in stainless steel. G-band corresponds to sp^2-bonded C–C stretching which is often witnessed from the honeycomb crystalline structure of graphitic samples.[14,25] The 2D and D + G peaks are related to the quality of the crystalline structure.[26] In this study, the D/G intensity ratio is used to describe the level of disorder in carbon deposits, and the bands of 2D and D + G are ignored. As shown in Fig. 3, the intensities of D-band and G-band were gradually decreased when the distance between the stainless steel and the inlet of tube increased from 0 to 20 cm, and tuned to increase with the increasing distance from 20 to 30 cm. The intensity of carbon deposition was highest at the distance of 5 cm. These results may be attributed to the disturbed flow region around the inlet and outlet of large pipeline of tube with sudden area expansion. The disturbed gas flow gives rise to high collision probability, resulting in more carbon formation near the inlet and outlet region.[27] In real industrial applications, prevention of the design of corners would be one effective strategy for reduction of the carbon deposition.

The heating temperature inside furnace could also influence the carbon deposition on stainless steel. To investigate the heating effect, the temperature was set in the range from 400 to 900 °C according to the real industrial production process. The stainless steel was put into the center of U-type quartz tube to reduce the deviations among each test. After introducing C_2H_4 at 30 mL h^{-1} for 30 min, the stainless steel was removed from the tube for Raman analysis. The signal intensities of D-band and G-band increased with the accelerated temperature from

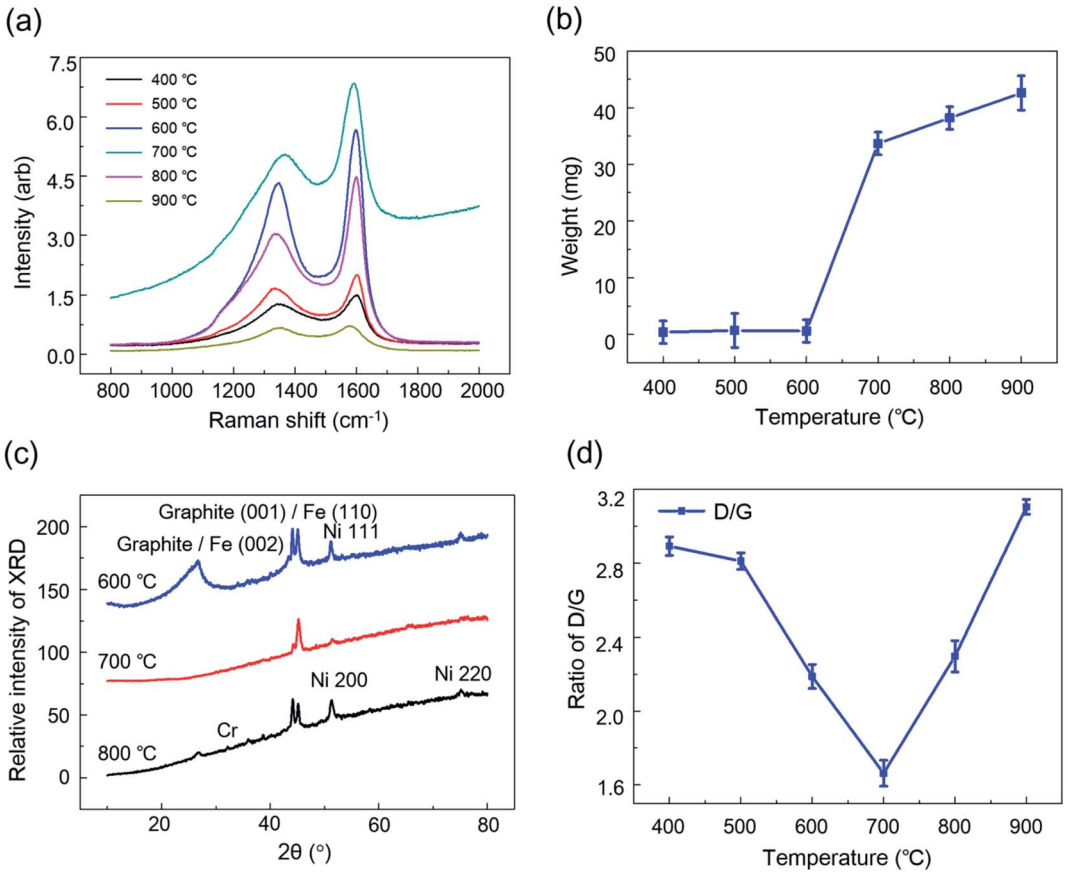

Fig. 4 Temperature effect on carbon deposition. (a) Raman spectra of temperature-dependent carbon deposition, (b) the weight of deposited carbon at different temperatures, (c) XRD analysis of deposited carbon on the stainless steel, and (d) the D/G intensity ratio.

400 to 700 °C, and gradually decreased from 700 to 900 °C (Fig. 4a). Moreover, the weight of carbon deposition on stainless steel *versus* the temperature showed a sigmoid growth curve. The weight of carbon deposition was below 5 mg for the temperature below 600 °C, while significantly increased to around 35 mg at 700 °C and gradually increased to around 45 mg with the higher temperature up to 900 °C (Fig. 4b). These results suggested that the activation temperature for carbon deposition was 700 °C in our system. To understand this temperature-modulated carbon deposition, we used XRD analysis to characterize the components of deposited complex. When the temperature was 600 °C, the complex contained graphite, Fe and Ni, indicating that carbon deposition was induced by Fe and Ni catalysis (Fig. 4c). When the temperature was 800 °C, Fe-catalyzed carbon deposition was greatly reduced. When the temperature was 700 °C, carbon deposition was solely depended on Fe catalyst.[28] Moreover, the high temperature of 700 °C simultaneously accelerated the diffusion rate of carbon atoms, as well as trigging the iron-catalyzed carbon deposition significantly, resulting in the formation of more carbon deposits than the lower temperature.[29,30] The temperature of 700 °C was beneficial for the formation of graphite deposition, indicated by the lowest D/G intensity ratio from Raman spectra (Fig. 4d). When increasing the temperature to 800 or 900 °C, the D/G intensity ratio was also increased, corresponding to the formation of more amorphous carbon than graphite in carbon deposits. Therefore, the temperature modulated both the diffusion rate of carbon atoms and the chemical surface reaction, playing a significant role in carbon deposition as well as the level of disorder in carbon deposits.

The flow rate of C_2H_4 is another important factor during carbon deposition because it directly affects the absorption and diffusion of C_2H_4 onto the surface of stainless steel. To study the flow rate-dependent carbon deposition, the piece of stainless steel was put at the center of U-shape quartz tube and heated for 30 min at 700 °C with different flow rates of C_2H_4 from 5 to 50 mL min^{-1}. As shown in Fig. 5, the intensity of carbon deposition increased with increasing the flow rate and achieved a maximum value at 50 mL min^{-1}. The high flow rate of C_2H_4 could result in the chaotic flow inside the tube, thus dramatically enhancing the interaction between C_2H_4 and the stainless steel and the subsequent carbon deposition. Thus, changing the flow rate of C_2H_4 could efficiently alter the carbon deposition. This phenomenon is also observed in position-effect experiments in which more carbon deposition is formed at the disturbed flow region.

3.2 Carbon deposition on acid treated stainless steel

Ethylene-involved processes often suffer from the harsh environments such as erosive flow and acidic conditions.[31] Establishment of a model of acid corrosion is vital for investigating the carbon deposition in ethylene-related applications. To do so, HCl solutions with different pH values as 1, 2, 3, 4, 5, 6 and 7 were prepared, and the pH values of HCl solutions were adjusted by 0.1 M NaOH solution. 3 pieces of 14 × 14 × 2 mm stainless steel (regarded as one group) were treated under one

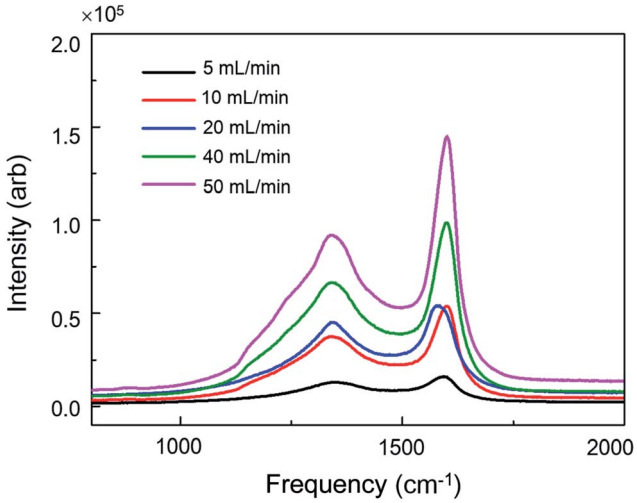

Fig. 5 The effect of flow rate of C_2H_4 on carbon deposition.

pH value. A total of 7 groups were treated by HCl solutions with different pH values from 1 to 7. Each piece of stainless steel, was submerged into HCl solution. The acid corrosion on the surface of stainless steel was carried out for 24 h. After acid treatment, the stainless steel was washed with DI water to remove acid solution and interferential soluble ions. Each group of acid-treated stainless steel was then put in the center of U-shape quartz tube at 700 °C with 50 mL min^{-1} of C_2H_4 for 30 min. 7 experimental runs were carried out for 7 groups of acid-treated samples. After treatment, the thickness of carbon deposition was decreased with the increased values of pH. The different thickness was correlated with the pH-dependent surface oxides that influenced the effective contact area of metal and gas. The weight of carbon deposits on the acid-treated stainless steel was showed in Fig. 6a. The carbon species deposited on acid-treated stainless steel was also analyzed by Raman spectroscopy. From Fig. 6b, we found that the Raman intensity of carbon deposition was increasing with the increase of pH value and reached a maximum point at pH = 4. The D/G intensity ratio indicating the ratio of disordered carbon to graphitic carbon was also changed with the increase of pH value (Fig. 6c). The SEM image of the surface of stainless steel showed that particle size of deposited carbon was fairly uniform with diameter of 3∼5 μm (Fig. 6d).[32–34]

To further analyze the carbon deposition on the acid-treated stainless steel, XPS with argon ion sputtering was used to characterize the chemical states of the surface of stainless steel after acid treatment. The surface state of stainless steel with exposed metal ions directly affected the pyrolytic decomposition of C_2H_4, which accelerating the formation of carbon deposition. XPS analysis displayed that Fe, Ni, Cr and their oxidation states were changed under acid treatment. Fe and Cr in oxidized states existed in acid-treated stainless steel regardless the pH values (Fig. 7). In comparison, Ni and its oxidation state only appeared on the surface of stainless steel treated with acid solution at pH = 1 and pH = 2 (Fig. 7). These results revealed that acid-treatment could alter the surface chemical of

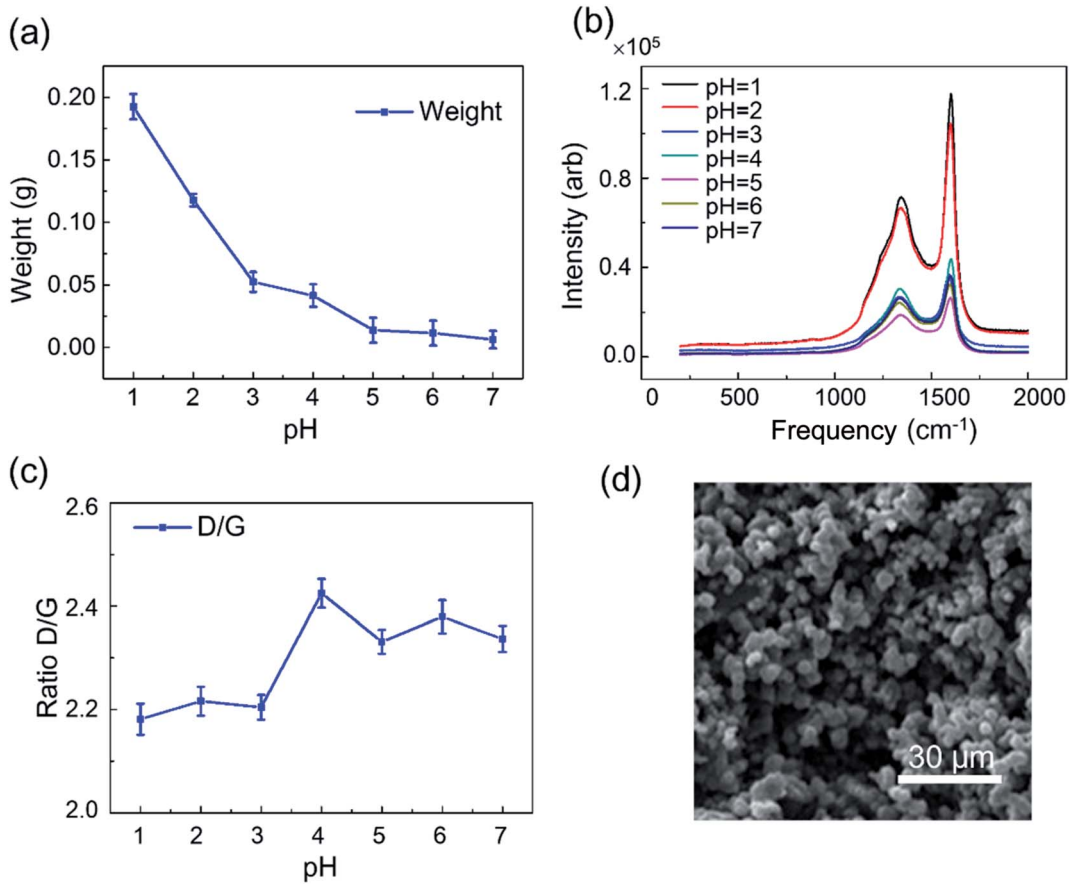

Fig. 6 Carbon deposition on stainless steel treated with acid solutions at different pH values. (a) The amount of deposited carbon with different pH treatment. (b) The Raman spectra of carbon deposition on acid-treated stainless steel at different pH values. (c) The plotting of the D/G intensity ratio at different pH values. (d) SEM image of the carbon particles on the acid-treated surface. The scale bar is 30 μm.

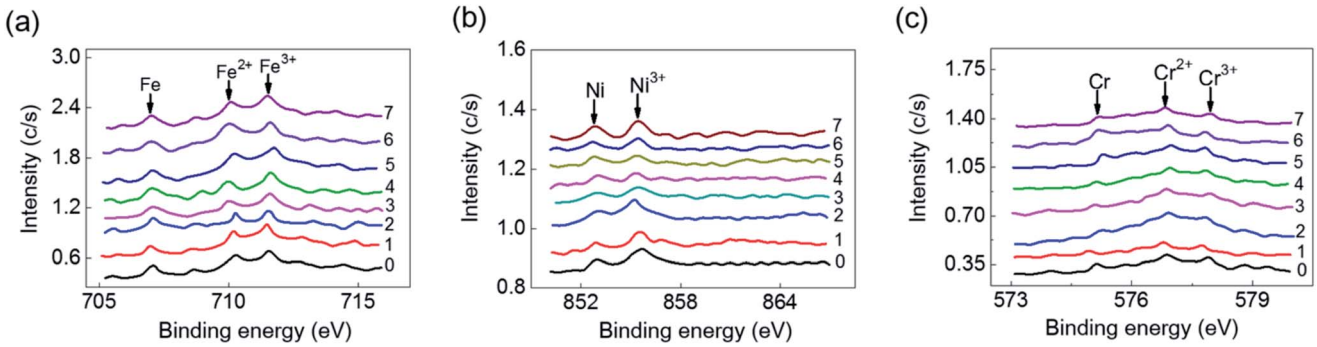

Fig. 7 XPS spectra of Fe (a), Ni (b), and Cr (c) on the surface of acid-treated stainless steel at different pH values.

stainless steel, resulting in the formation of more carbon deposition with the increase of acidity. To efficiently reduce the carbon deposition, the acid-treatment of metal should be avoided. The results demonstrated that acidic treatment of metal surfaces led to the increased carbon deposition due to the larger contact area between metal and gas, resulting in the formation of additional metal carbides. Also, the acidic environment and collisions should be avoided as much as possible during the process of the production and application of ethylene.

4. Conclusions

In this study, we focused on the investigation of carbon deposition during the production and application of ethylene. Raman spectroscopy has been used to map and monitor different carbon species under different conditions. When the temperature was low, the rate-limiting step for carbon deposition was the metal surface chemical reaction. With the elevated temperature, carbon diffusion was the rate-limiting step. Moreover, acid corrosion of the metal surface resulted in large

effective contact areas of gas and metals, leading to increased carbon deposition. Fe, Ni, Cr and their oxidation states were also monitored by XPS after carbon deposition. This work provided a simple and rapid method for studying the carbon deposition, which is potentially useful for prevention of undesired carbon deposition in the process of industrial processes.

Acknowledgements

This work was supported by the National Natural Science Foundation of China (No. 21435002, 81373373, 21621003), and Beijing Municipal Science and Technology Commission (Z171100001117135, Z161100004916095).

References

1 M. Kogler, E.-M. Köck, B. Klötzer, T. Schachinger, W. Wallisch, R. Henn, C. W. Huck, C. Hejny and S. Penner, *J. Phys. Chem. C*, 2016, **120**, 1795–1807.
2 S. Yoon, I. Kang and J. Bae, *Int. J. Hydrogen Energy*, 2009, **34**, 1844–1851.
3 A. C. Koeken, T. Galvis, M. Hirsa, T. Davidian, M. Ruitenbeek and K. P. De Jong, *Angew. Chem., Int. Ed.*, 2012, **51**, 7190–7193.
4 V. Varshney, J. Lee, D. Li, J. S. Brown, B. L. Farmer, A. A. Voevodin and A. K. Roy, *Carbon*, 2017, **114**, 15–22.
5 R. González-Gil, I. Chamorro-Burgos, C. Herrera, M. Larrubia, M. Laborde, F. Marino and L. Alemany, *Int. J. Hydrogen Energy*, 2015, **40**, 11217–11227.
6 X. Yang, G. Gao, Q. Shi, X. Wang, J. Zhang, C. Han, J. Wang, H. Lu, J. Liu and M. Tong, *Int. J. Hydrogen Energy*, 2014, **39**, 3231–3242.
7 J. Gao, Y. Wang, Y. Ping, D. Hu, G. Xu, F. Gu and F. Su, *RSC Adv.*, 2012, **2**, 2358–2368.
8 S. Mattioli, M. Peltzer, E. Fortunati, I. Armentano, A. Jiménez and J. M. Kenny, *Carbon*, 2013, **63**, 274–282.
9 M. S. Dresselhaus and G. D. Jorio, *J. Phys. Chem. C*, 2007, **111**, 17887–17893.
10 J. Kuhn and O. Kesler, *J. Power Sources*, 2014, **246**, 430–437.
11 K. S. Blinn, H. Abernathy, X. Li, M. Liu, L. A. Bottomley and M. Liu, *Energy Environ. Sci.*, 2012, **5**, 7913–7917.
12 J. Li, Z. Zhu, B. Zhu, Y. Ma, B. Lin, R. Liu, Y. Song, H. Lin, S. Tu and C. Yang, *Anal. Chem.*, 2016, **88**, 7828–7836.
13 Y. Zhang, W. Zhou, Y. Xue, J. Yang and D. Liu, *Anal. Chem.*, 2016, **88**, 12502–12507.
14 R. Maher, V. Duboviks, G. Offer, M. Kishimoto, N. Brandon and L. Cohen, *Fuel Cells*, 2013, **13**, 455–469.
15 J. Ribeiro-Soares, M. Oliveros, C. Garin, M. David, L. Martins and C. Almeida, *Carbon*, 2015, **95**, 646–652.
16 Y. Zhang, Y. L. Zhang and C. W. Zhou, *Acc. Chem. Res.*, 2013, **46**, 2329–2339.
17 S.-K. Joung, T. Okazaki, S. Okada and S. Iijima, *J. Phys. Chem. C*, 2012, **116**, 23844–23850.
18 P. E. Oliveira, L. P. Ribeiro, M. G. Rosmaninho, J. D. Ardisson, A. Dias, L. C. Oliveira and R. M. Lago, *Catal. Commun.*, 2013, **32**, 58–61.
19 B. Hua, M. Li, B. Chi and L. Jian, *J. Mater. Chem. A*, 2014, **2**, 1150–1158.
20 T. Matsui and K. Eguchi, *Carbon*, 2015, **85**, 444.
21 A. Page, F. Ding, S. Irle and K. Morokuma, *Rep. Prog. Phys.*, 2015, **78**, 036501.
22 V. Jourdain and C. Bichara, *Carbon*, 2013, **58**, 2–39.
23 L. Dimesso, C. Förster, W. Jaegermann, J. Khanderi, H. Tempel, A. Popp, J. Engstler, J. Schneider, A. Sarapulova and D. Mikhailova, *Chem. Soc. Rev.*, 2012, **41**, 5068–5080.
24 E.-X. Ding, H.-Z. Geng, W.-Y. Wang, L. Mao, Y. Wang, Z.-C. Zhang, Z.-J. Luo, J. Wang, H.-J. Yang and L. Pan, *Carbon*, 2015, **82**, 604–607.
25 W. Qiu, Q. Li, Z.-K. Lei, Q.-H. Qin, W.-L. Deng and Y.-L. Kang, *Carbon*, 2013, **53**, 161–168.
26 A. C. Ferrari and D. M. Basko, *Nat. Nanotechnol.*, 2013, **8**, 235–246.
27 E. Kukovitsky and S. Lvov, *ECS J. Solid State Sci. Technol.*, 2013, **2**, M1–M8.
28 J. Riquelme, C. Garzón, C. Bergmann, J. Geshev and R. Quijada, *Eur. Polym. J.*, 2016, **75**, 200–209.
29 R. Trane-Restrup and A. D. Jensen, *Appl. Catal., B*, 2005, **165**, 117–127.
30 P. Liu, W. Xing, X. Cheng, D. Li, Y. Li and X.-Q. Chen, *Phys. Rev. B: Condens. Matter Mater. Phys.*, 2014, **90**, 024103.
31 T. J. Schwartz, R. L. Johnson, J. Cardenas, A. Okerlund, N. A. Da Silva, K. Schmidt-Rohr and J. A. Dumesic, *Angew. Chem.*, 2014, **126**, 12932–12936.
32 A. Sacco, F. W. A. H. Geurts, G. A. Jablonski, S. Lee and R. A. Gately, *J. Catal.*, 1989, **119**, 322–341.
33 G. A. Jablonski, F. W. Geurts, A. Sacco and R. R. Diederman, *Carbon*, 1992, **30**, 87–98.
34 W. Y. Li, Y. X. Shi, Y. Luo, Y. Q. Wang and N. S. Cai, *J. Power Sources*, 2015, **276**, 26–31.